A Reciprocal Heuristic Model for Diffuse Scattering From Walls and Surfaces

Enrico M. Vitucci, *Senior Member, IEEE*, Nicolò Cenni, Franco Fuschini, and Vittorio Degli-Esposti, *Senior Member, IEEE*

***Abstract*— Diffuse scattering (DS) of electromagnetic waves from natural and artificial surfaces has been extensively studied in various disciplines, including radio wave propagation, and several DS models based on different approaches have been proposed over the years, two of the most popular ones being Kirchhoff theory and the so-called effective roughness (ER) heuristic model. The latter, although less rigorous than the former, is more flexible and applicable to a wider range of real-world cases, including non-Gaussian surfaces, surfaces with electrically small correlation lengths and scattering from material inhomogeneities that are often present under the surface. Unfortunately, the ER model, with the exception of its Lambertian version, does not satisfy reciprocity, which is an important physical-soundness requirement for any propagation model. In the present work, without compromising its effectiveness and its simple and yet sound power-balance approach, we propose a reciprocal version of the ER model, which can be easily implemented and can replace the old version in ray-based propagation models. The new model is analyzed and compared with the old one and with other popular models. Once properly calibrated, it is shown to yield similar—if not better—performance with respect to the old one when checked versus measurements.**

***Index Terms*— Building walls, diffuse scattering (DS), field reciprocity, irregular surfaces, power conservation, radio frequency (RF) coverage, radio propagation, ray tracing.**

I. Introduction

DIFFUSE scattering (DS) of radio waves, intended here as nonspecular reflection from terrain, objects, and building walls' surfaces due to surface roughness or material irregularities, has been studied for years in many application fields such as remote sensing and optics.

Manuscript received 4 September 2022; revised 7 March 2023; accepted 12 May 2023. Date of publication 26 May 2023; date of current version 7 July 2023. This work was supported in part by the European Union through the Italian National Recovery and Resilience Plan (NRRP) of NextGenerationEU, partnership on "Telecommunications of the Future"- Programme "RESearch and innovation on future Telecommunications systems and networks to make Italy more smART (RESTART)", under Grant PE00000014; in part by the EU Project 6G SHort range extreme communication IN Entities (6G-SHINE), Horizon Europe Program, under Grant 101095738; and in part by the European Cooperation in Science and Technology (COST) Action "Intelligence-Enabling Radio Communications for Seamless Inclusive Interactions" (INTERACT), under Grant CA20120. *(Corresponding author: Enrico M. Vitucci.)*

The authors are with the Department of Electrical, Electronic, and Information Engineering "Guglielmo Marconi" (DEI), CNIT, University of Bologna, 40126 Bologna, Italy (e-mail: enricomaria.vitucci@unibo.it; nicolo.cenni2@unibo.it; franco.fuschini@unibo.it; v.degliesposti@unibo.it).

Color versions of one or more figures in this article are available at https://doi.org/10.1109/TAP.2023.3278796.

Digital Object Identifier 10.1109/TAP.2023.3278796

With reference to radio propagation in urban environment, assuming flat, smooth, and homogeneous building walls or indoor furniture panels, propagation can be conveniently analyzed using the geometrical optics (GO) approximation [1], where radio wave interactions can be modeled as specular reflections, transmissions, and edge diffractions.

However, perfectly smooth slabs are rarely present in real life, especially in dense urban areas where building walls can show relevant deviations from smooth homogeneous layers, such as compound materials, window frames, metal reinforcements, pillars, rough plaster and brick surfaces, cables, and advertising boards. Similar considerations hold true for indoor walls and furniture. In fact, some investigations showed that DS due to such details—often disregarded in building maps and databases—can be an important propagation mechanism in urban environment [2], [3], [4], [5]. In particular, DS has been shown to generate a large part of the time-domain, angle-domain, and polarization dispersion of the multipath radio channel in most environments [6], [7], [8], [9], and the knowledge of this phenomena can be exploited in the design of MIMO wireless links and to implement advanced beamforming strategies [10], [11], [12]. Moreover, DS has been shown to play a prominent role even in the determination of the actual radio frequency (RF) coverage level, especially in non-line of sight (NLoS), millimeter-wave frequency applications [13]. Recent studies have also highlighted the importance of DS from rough surfaces in terahertz wireless communications links [14], [15], [16]. Therefore, accounting for specular reflection, transmission, and diffraction is not sufficient: analysis and modeling of DS is mandatory to achieve a complete understanding of urban radio propagation.

The most widely known DS models available in the literature only deal with surface roughness and include Kirchhoff theory, the small perturbation method, and the integral equation method [17], [18]. The most popular approach to DS is the Kirchhoff theory, based on the Beckmann–Kirchhoff theory for scattering of incident plane waves from Gaussian rough surfaces described in terms of roughness standard deviation and correlation distance [17]. Another DS approach developed specifically for building walls and derived from physical optics is proposed in [19]: here, the assumption is that nonspecular scattering from the façades of large buildings is dominated by windows and decorative masonry, whose placement tends to be nearly periodic.

However, Kirchhoff theory is not applicable to non-Gaussian surface roughness, to strong surface irregularities where the roughness correlation length is comparable to, or smaller than, the wavelength (e.g., indentations), or when the surface size is comparable to, or smaller than, correlation length. Moreover, all the cited models are not suitable to cases where the presence of internal, material irregularities have a significant impact. The possibility for radio waves to penetrate inside the wall, undergo scattering interactions due to the internal inhomogeneities, and re-emerge with nearly random propagation direction and characteristics must also be accounted for.

Therefore, in more recent years heuristic models such as the effective roughness (ER) model [4] have been proposed to overcome the foregoing limitations. The ER model is aimed at modeling nonspecular scattering from surfaces, but its parameters are not actual surface roughness parameters as for the Kirchhoff model, they are "effective" parameters that must take into account also the effect of the more general irregularities and details described above, hence the name "ER" model. Thanks to its heuristic nature, the ER model can account for the effect of any kind of surface or volume inhomogeneity, without restriction with respect to its statistical characteristics. Differently from the Kirchhoff model, the specular reflected wave and the scattered wave are treated from the beginning as distinct waves where the attenuation of the former is due to part of its power being diverted into the latter by irregularities. This fact allows its straightforward, "plug-and-play" integration into the ray-based models where specular reflection and transmission are implemented as phase-coherent waves that follow the GO theory, albeit with a proper attenuation, while DS can have different spatial and polarization characteristics.

The ER model is physically consistent as it is based on a power balance between specular reflection, transmission, and scattering. It is flexible because the scattering pattern can be chosen among several different options, and due to its simplicity and low number of parameters it can be easily tuned versus measurement data.

After its introduction in 2007, analytical formulations of the ER model have been developed to describe the angle spread produced by DS from a single wall [20]; it has been extended to transmitted scattering in the forward half-space (e.g., beyond a wall) [21] and has been further validated versus full-wave electromagnetic simulations and measurements in reference cases [22]. The parameterization of the ER model in the mm-wave bands for different construction materials has also been discussed in [23] and [24]. Furthermore, the ER model has been finally embedded into some commercial ray-based field prediction software tools [25].

Despite its strengths, the original—or legacy—ER model also has an important shortcoming: with the exception of its Lambertian scattering pattern version, it does not fully satisfy reciprocity, which means that the predicted scattered field intensity is not invariant with respect to the exchange of the transmitter and receiver, as it should be according to the propagation theory [26]. Although, being a heuristic model, its fitting to the actual physical process can always be adjusted through parameter calibration, nonreciprocity represents an important theoretical flaw, especially considering that its nonreciprocal, directive scattering versions have been shown to be the most suitable to describe DS from real buildings [4].

Other models similar to the ER model that satisfy reciprocity have been developed for computer graphic applications [27], [28], or have been derived from them [29]. However, such models do not distinguish specular from diffuse reflection and therefore cannot be easily implemented into the existing ray-based propagation models. Moreover, although power constraints are present, such as that the backscattered power cannot be greater than the incident power, they do not comply with a clear power conservation balance at the surface to minimize parameters and to achieve maximum compatibility with the traditional formulations based on GO for smooth surfaces and material slabs.

In the present work, starting from the approach of the original ER model, we first develop a better and more complete mathematical derivation of its normalization factors with respect to the rather incomplete demonstration provided in [4], using Euler's Gamma and Beta functions. Then we propose a new version of the ER model that satisfies reciprocity without sacrificing the original power-balance assumptions, if not to a negligible extent for grazing incidence. We also provide a discussion on reciprocity and power balance of the new ER model with respect to the original formulation and a comparison with respect to other reference models (e.g., Kirchhoff). Finally, the model is validated through comparison with measurements in a reference case.

This article is organized as follows. In Section II, some background on the original ER model and its formulation are provided, and then the new reciprocal formulation is presented (the mathematical details are provided in the appendices). In Section III, comparisons to the legacy ER model, to other reference models, and to measurements are shown and discussed. Finally, conclusions are drawn in Section IV.

II. New ER Model's Formulation

A. Background on the ER Model

When a surface element dS is illuminated by an impinging electromagnetic wave, the following power balance must hold:

$$P_i = P_r + P_s + P_p \tag{1}$$

with P_i, P_r, P_s, and P_p being the incident, the reflected, the scattered, and transmitted powers, respectively (see Fig. 1).

The basic assumption of the ER approach is that the scattered power can be simply related to a scattering coefficient $S \in [0, 1]$ as

$$P_s = S^2 \cdot \left(U^2 P_i\right). \tag{2}$$

Depending on the value of U, S^2 represents the percentage of either the incident ($U = 1$) or the reflected power ($U = \Gamma$, being $\Gamma = |\bar{E}_r|/|\bar{E}_i|$ the modulus of the reflection coefficient) that is spread in nonspecular directions [4]. In the following, DS is supposed to occur at the expense of specular reflection, i.e., $U = \Gamma$ is considered in (2).

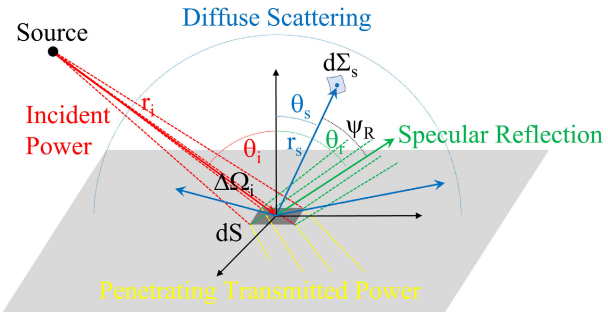

Fig. 1. Power balance on a surface element: incident wave, specular reflection, DS, and penetrated power.

Therefore, the power balance (1) can be written as

$$1 = \Gamma^2 R^2 + \Gamma^2 S^2 + P_p/P_i \tag{3}$$

where R is the reflection reduction factor, which is related to the so-called "Rayleigh's factor" of the Kirchhoff theory [17]. By assuming that the ratio P_p/P_i does not depend on the degree of roughness, i.e., on the parameter S, from (3) we easily get that the reflection reduction factor is [4]: $R = \sqrt{1 - S^2}$.

The power-balance assumptions of the legacy ER model (referred to as *ER power balance* in the following), represented by (2) and (3), imply the following equation where the power diverted from specular reflection equals the integral of the scattered field power density over the backscattering half-space, i.e. (see Fig. 1):

$$\begin{aligned} P_s &= S^2\Gamma^2 P_i = S^2\Gamma^2 \frac{|\bar{E}_i|^2}{2\eta}\Delta\Omega_i\, r_i^2 \\ &= \int_0^{2\pi}\int_0^{\frac{\pi}{2}} \frac{|\bar{E}_S|^2}{2\eta} r_S^2 \sin\theta_S\, d\theta_S\, d\phi_S \end{aligned} \tag{4}$$

where r_i and r_S are the distances between the surface element dS and the source, and between dS and the observation point, respectively, $\Delta\Omega_i$ is the solid angle subtended from dS at the transmitter side (see Fig. 1), and $\eta = \sqrt{\mu_0/\epsilon_0}$ is the free-space impedance.

Moreover, the squared amplitude of the scattered field is assumed to be expressed by the following formula:

$$\left|\bar{E}_S(\theta_i, \phi_i, \theta_S, \phi_S)\right|^2 = E_{S0}^2 \cdot\ f(\theta_i, \phi_i, \theta_S, \phi_S) \tag{5}$$

where $f(\theta_i, \phi_i, \theta_S, \phi_S) \in [0, 1]$ represents the DS spatial pattern. The overall scattered field is then modeled as a nonuniform spherical wave.

Assuming the surface element dS in the far-field region of the transmitting source, the incident field is a spherical wave, and therefore,

$$\left|\bar{E}_i(r_i, \theta_i, \phi_i)\right| = \frac{\sqrt{60\ P_t\ g_t(\theta_i, \phi_i)}}{r_i} = \frac{K_i(\theta_i, \phi_i)}{r_i} \tag{6}$$

where $K_i(\theta_i, \phi_i)$ is a parameter depending on the source properties (transmit power, antenna gain). By substituting (5) and (6) into (4) and exploiting the expression for the solid angle $\Delta\Omega_i = ((dS\cos\theta_i)/r_i^2)$, the following formula can be achieved:

$$|\bar{E}_S|^2 = \underbrace{\frac{\left(\frac{K_i S}{r_i r_S}\right)^2 \Gamma^2\, dS\, \cos\theta_i}{F(\theta_i, \phi_i)}}_{E_{S0}^2} \cdot f(\theta_i, \phi_i, \theta_S, \phi_S) \tag{7}$$

where $F(\theta_i, \phi_i)$ represents the following integral expression:

$$F(\theta_i, \phi_i) = \int_0^{2\pi}\int_0^{\frac{\pi}{2}} f(\theta_i, \phi_i, \theta_S, \phi_S) sin\,\theta_S\, d\theta_S\, d\phi_S. \tag{8}$$

It can be observed that according to (7), $|\bar{E}_S| = 0$ for any observation angle, when the incident wave is parallel to the surface element, i.e., $\theta_i = \pi/2$: in fact, for grazing incidence, no power is captured and then scattered by the surface.

It is worth noting that to have a reciprocal expression for the intensity of the scattered field $|\bar{E}_S|$, the product of the three functions in (7) needs to be reciprocal, i.e.,

$$\frac{f(\theta_i, \phi_i, \theta_S, \phi_S)}{F(\theta_i, \phi_i)} \cdot cos\,\theta_i = g_{rec}(\theta_i, \phi_i, \theta_S, \phi_S) \tag{9}$$

where g_{rec} is a reciprocal function, i.e., a function invariant to the exchange of (θ_i, ϕ_i) with (θ_S, ϕ_S).

The former version of the scattering model in [4] was aimed at a single-lobe, directive scattering pattern by means of the following choice:

$$f(\theta_i, \phi_i, \theta_S, \phi_S) = \left(\frac{1 + \cos\psi_R}{2}\right)^{\alpha_R} \quad \alpha_R \in \mathbb{N} \tag{10}$$

where the integer exponent α_R is a tuning parameter for the directivity of the scattering pattern (the greater the α_R, the narrower the lobe), and ψ_R is the angle between the scattering direction (θ_S, ϕ_S) and the specular direction (see Fig. 1). The following relation is also provided in [4]:

$$\cos\psi_R = \cos\theta_i \cos\theta_S - \sin\theta_i \sin\theta_S \cos(\phi_S - \phi_i). \tag{11}$$

By applying the power balance (4), (7) becomes

$$|\bar{E}_S|^2 = \left(\frac{K_i S}{r_i\, r_S}\right)^2 \Gamma^2 \frac{dS\, \cos\theta_i}{F_{\alpha_R}(\theta_i)} \left(\frac{1 + \cos\ \psi_R}{2}\right)^{\alpha_R} \tag{12}$$

where F_{α_R} is the solution of the integral in (8), when (10) is enforced [4]. Note that with the chosen shape for the scattering pattern in (10), F_{α_R} does not depend on the azimuth angle ϕ_i, for symmetry reasons.

A complete solution for F_{α_R} was not derived in [4]: however, two different, closed-form expressions were proposed, depending on whether α_R is even or odd.

Instead, a more compact and general expression for F_{α_R} is fully derived in this work, by exploiting the properties of Euler's Beta function (Appendix A). The new closed-form solution valid for any value of α_R is (see Appendix B)

$$\begin{aligned} F_{\alpha_R}(\theta_i) = \frac{2\pi\ \alpha_R!}{2^{\alpha_R}} &\sum_{j=0}^{\alpha_R} \frac{1}{(\alpha_R - j)!(j+1)!!} \\ &\cdot \sum_{l=0}^{\lfloor j/2 \rfloor} \frac{\cos^{j-2l}\theta_i \sin^{2l}\theta_i}{2^l\, l!(j-2l)!!} \quad 0 \le \theta_i < \frac{\pi}{2} \end{aligned} \tag{13}$$

where $\lfloor x \rfloor$ stands for the greatest integer less than or equal to x, and ! and !! symbols stand for the factorial and double

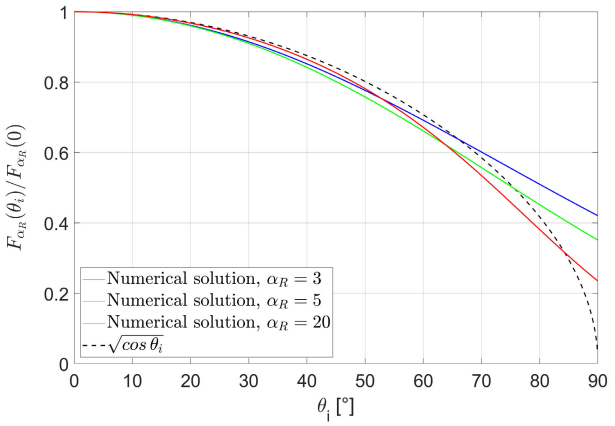

Fig. 2. Comparison of the function $\sqrt{\cos\theta_i}$ with $F_{\alpha_R}(\theta_i)$, for different values of the exponent α_R.

factorial functions, respectively (see Appendix A). In the case of normal incidence ($\theta_i = 0$), (13) reduces to

$$F_{\alpha_R}(0) = \frac{4\pi}{\alpha_R + 1}\left(1 - \frac{1}{2^{\alpha_R+1}}\right).$$

Looking at (12) and (13), it is evident that the amplitude of the scattered field $|\bar{E}_S|^2$ is nonreciprocal, due to the presence in (13) of the functions $(\cos\theta_i)^m$ and $(\sin\theta_i)^m$, which are not counterbalanced by similar terms containing the scattering elevation angle θ_S.

B. New Reciprocal Formulation

The aim is to achieve a reciprocal expression for the scattered field. To this extent, we propose the following new expression for the DS pattern:

$$f(\theta_i, \phi_i, \theta_S, \phi_S) = \sqrt{\cos\theta_S}\left(\frac{1 + \cos\psi_R}{2}\right)^{\alpha_R} \quad \alpha_R \geq 1. \quad (14)$$

Such scattering function is obtained by multiplying the pattern of the legacy ER model, i.e., (10), by the factor $\sqrt{\cos\theta_S}$. With this assumption, the scattered power tends to zero for grazing observation angles, i.e., when θ_S approaches $\pi/2$. This is a necessary condition for reciprocity: in fact, according to (7), $|\bar{E}_S| = 0$ for $\theta_i = \pi/2$, no matter what is the observation angle θ_S as the solid angle $\Delta\Omega_i$ goes to zero; similarly, it must be $|\bar{E}_S| = 0$ for $\theta_S = \pi/2$, independently of the incidence angle θ_i.

Besides, it can be observed that the multiplication of (10) by $\sqrt{\cos\theta_S}$ causes a skew of the maximum of the scattering pattern with respect to specular reflection. This misalignment is of the order of a few degrees and is more evident for grazing incidence angles and low values of the parameter α_R: some examples will be shown and discussed in Section III.

Let us now discuss more in detail the reciprocity of the new model's formulation. For the model to be reciprocal, according to (9), the following condition must be satisfied:

$$\frac{\cos\theta_i}{F_{\alpha_R}} \propto \sqrt{\cos\theta_i} \quad (15)$$

which implies $F_{\alpha_R} \propto \sqrt{\cos\theta_i}$.

Actually, it can be observed that F_{α_R} that would result from (14) being inserted into (8), i.e., which satisfies *ER power balance*, is a monotonic decreasing function having its maximum value for $\theta_i = 0$, which can be well approximated by a function proportional to $\sqrt{\cos(\theta_i)}$, as shown in Fig. 2. This means that if we assume $F_{\alpha_R} \propto \sqrt{\cos(\theta_i)}$, reciprocity is strictly satisfied, while also *ER power balance* is satisfied to a good extent.

In fact, Fig. 2 shows $F_{\alpha_R}(\theta_i)/F_{\alpha_R}(0)$ derived from (8) through numerical integration for three different values of the parameter α_R, versus the function $\sqrt{\cos\theta_i}$. It can be observed that the approximation is very good except for very grazing incidence angles (e.g., greater than 85°). This allows to write F_{α_R} in the form

$$F_{\alpha_R}(\theta_i) \approx k(\alpha_R)\sqrt{\cos\theta_i} \quad (16)$$

where $k(\alpha_R)$ is an amplitude parameter depending only on the exponent α_R. This approximation satisfies both (9) (i.e., reciprocity) and, with good approximation, (8) (i.e., *ER power balance*).

The value of $k(\alpha_R)$ can be determined in a straightforward way by assuming the approximation (16) as valid and solving the integral (8) for $\theta_i = 0$, as shown in Appendix C.

Then, the final reciprocal expression of the scattered field when (14) is enforced and under the approximation (16) is (see Appendix C)

$$|\bar{E}_S|^2 = \left(\frac{K_i S}{r_i\, r_S}\right)^2 \Gamma^2 \frac{dS}{k(\alpha_R)} \cdot \sqrt{\cos\theta_i \cos\theta_S}\left(\frac{1 + \cos\psi_R}{2}\right)^{\alpha_R} \quad (17)$$

with

$$k(\alpha_R) = \frac{4\pi}{2^{\alpha_R}} \sum_{j=0}^{\alpha_R} \binom{\alpha_R}{j} \frac{1}{2j+3}.$$

The expression used in (17) for $k(\alpha_R)$ is valid only for integer positive values of the exponent α_R, as it has been computed using the binomial theorem (see Appendix C). However, in case real positive values of the exponent α_R are needed for a finer tuning of the model, $k(\alpha_R)$ can be calculated using the following interpolating function:

$$k(\alpha_R) \approx \begin{cases} (0.07937\alpha_R + 0.1745)^{-1} & \text{if } \alpha_R > 4 \\ (0.002966\alpha_R^2 + 0.05675\alpha_R & \\ \quad + 0.2387)^{-1} & \text{if } 1 \leq \alpha_R \leq 4. \end{cases}$$

C. Double-Lobe Model, Reciprocal Formulation

Similar to what is done in [4] for the legacy ER model, it is possible to derive a double-lobe model, where an additional lobe steered in the incidence direction is added to the scattering pattern. This is useful in many practical cases, where walls with big irregularities, e.g., indentations, generate a strong backscattering component in the incidence direction through micro interactions consisting of multiple-bounce reflections (see Fig. 3).

To obtain a reciprocal formulation for this double-lobe model, we propose the following expression for the scattered

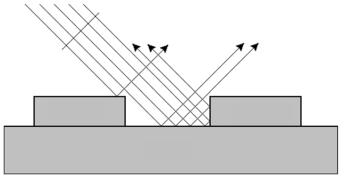

Fig. 3. Wall with indentations that generate a backscattering component in the incidence direction.

field:

$$|\bar{E}_S|^2 = \left(\frac{K_i S}{r_i\, r_S}\right)^2 \Gamma^2 \frac{dS\cos\theta_i}{F_{\alpha_i,\alpha_R}} \sqrt{\cos\theta_S} \cdot \left[\Lambda\left(\frac{1+\cos\psi_R}{2}\right)^{\alpha_R} + (1-\Lambda)\left(\frac{1+\cos\psi_i}{2}\right)^{\alpha_i}\right] \tag{18}$$

with

$$\begin{aligned} F_{\alpha_i,\alpha_R} &= \Lambda F_{\alpha_R} + (1-\Lambda) F_{\alpha_i} \\ F_{\alpha_R} &= \int_0^{2\pi}\int_0^{\frac{\pi}{2}} \sqrt{\cos\theta_S}\left(\frac{1+\cos\psi_R}{2}\right)^{\alpha_R} \sin\theta_S d\theta_S d\phi_S \\ F_{\alpha_i} &= \int_0^{2\pi}\int_0^{\frac{\pi}{2}} \sqrt{\cos\theta_S}\left(\frac{1+\cos\psi_i}{2}\right)^{\alpha_i} \sin\theta_S d\theta_S d\phi_S \end{aligned} \tag{19}$$

where ψ_i is the angle formed by the observation and incidence directions, α_i is a parameter that accounts for the directivity of the backscattering lobe, F_{α_i,α_R} is the solution of the power-balance integral (8) for the double-lobe pattern, and $\Lambda \in [0, 1]$ is a factor taking into account how the scattered power is subdivided between the two lobes.

It can be easily seen (see Appendix D) that both the integrals in (19) can be approximated by a function proportional to $\sqrt{\cos\theta_i}$, i.e., $F_{\alpha_R} \approx k(\alpha_R)\sqrt{\cos\theta_i}$ and $F_{\alpha_i} \approx k(\alpha_i)\sqrt{\cos\theta_i}$. If so, also F_{α_i,α_R} is proportional to $\sqrt{\cos\theta_i}$, and this allows to get a reciprocal expression for the scattered field. The final (reciprocal) expression of the scattered field for the double-lobe ER model is then

$$|\bar{E}_S|^2 = \left(\frac{K_i S}{r_i\, r_S}\right)^2 \Gamma^2 \frac{dS}{4\pi} \sqrt{\cos\theta_i\,\cos\theta_S} \cdot \left[\Lambda \frac{2^{\alpha_R}}{\sum_{j=0}^{\alpha_R}\binom{\alpha_R}{j}\frac{1}{2j+3}}\left(\frac{1+\cos\psi_R}{2}\right)^{\alpha_R} + (1-\Lambda)\frac{2^{\alpha_i}}{\sum_{j=0}^{\alpha_i}\binom{\alpha_i}{j}\frac{1}{2j+3}}\left(\frac{1+\cos\psi_i}{2}\right)^{\alpha_i}\right]. \tag{20}$$

Note also that (17) is obtained as a particular case of (20), when $\Lambda = 1$.

III. Comparisons

A. Comparison With Existing Models

The new, reciprocal ER model (RER model in the following) is discussed and compared with the legacy ER model and other models in this section.

The shape of its scattering pattern lobe is shown in Fig. 4 for different incidence angles and α_R values. The lobe's directivity increases with α_R, as it should, and its maximum is directed toward the specular direction. However, differently from the legacy ER model, the lobe is always constrained to have a null for $\theta_S = \pi/2$ to satisfy reciprocity as explained in Section II-B. Consequently, a slight drifting of the peak away from the specular direction toward lower θ_S values can be observed for incidence angles greater than $\pi/3$ and low α_R values.

As stated above, the new formulation of the ER model was derived to satisfy reciprocity. The original ER model, however, was already almost reciprocal for not-too-grazing incidence angles (up to about 40°), and for low values of α_R, as shown in Fig. 5, where the term $\cos\theta_i / F_{\alpha_R}(\theta_i, \phi_i)$ of (9) is almost constant, and therefore, reciprocity condition is approximately satisfied. On the other hand, it strictly respects the ER power balance, based on which it was conceived.

Conversely, the new ER model is perfectly reciprocal but its reciprocal formulation was obtained from an approximation that slightly differs from the numerical solution of the power-balance integral (8), especially for very grazing angles of incidence, as explained in Section II-B. It is worth noting, however, that reciprocity is a more important requirement than ER power balance, since the latter is based on the simplifying yet reasonable assumption that the quantity P_p/P_i of (3) does not depend on parameter S, which might not be rigorously true in real-life cases.

To quantify the influence of the approximation in the power-balance integral (8), we can introduce the *power-balance anomaly*, which is normalized to the incident power P_i and defined as

$$\Delta_{rel} = \frac{\hat{P}_s - P_s}{P_i} \tag{21}$$

where P_s is the scattered power obtained through the original power balance assumptions, i.e., through solution of the integral (8) to determine the value of $F_{\alpha_R}(\theta_i)$, while $\hat{P}_s$ is the corresponding value obtained using the approximation $F_{\alpha_R}(\theta_i) \approx k(\alpha_R)\sqrt{\cos\theta_i}$.

Through a few simple mathematical steps, the following expression for Δ_{rel} can be derived:

$$\Delta_{rel} = S^2\Gamma^2\left(\frac{F_{\alpha_R}(\theta_i)}{k(\alpha_R)\sqrt{\cos\theta_i}} - 1\right). \tag{22}$$

The power-balance anomaly Δ_{rel} of the new ER model is plotted versus θ_i in Fig. 6, assuming $S = 0.4$, while the modulus of the reflection coefficient Γ was calculated with the Fresnel coefficient (TE polarization) for the case of a lossless dielectric wall with $\epsilon_r = 5$. It is evident that Δ_{rel} is very small, within 1% of the incident power up to incident angles of 85° or more!

It is interesting to compare the behavior of the RER model with other models available in the literature, e.g., the Kirchhoff model for scattering from rough surfaces. The Kirchhoff model is a widely used reference model that, being physics-based, is reciprocal and necessarily satisfies physically consistent power-balance constraints. However, it has several parameters,

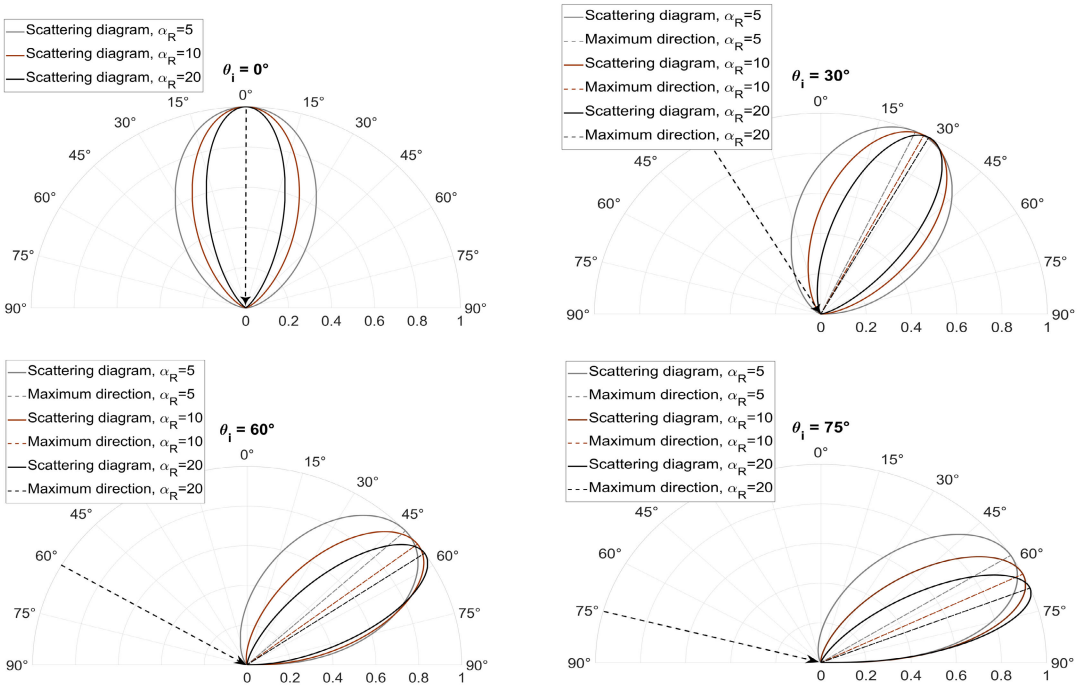

Fig. 4. Scattering patterns of the new RER model, for different incidence angles and values of the parameter α_R.

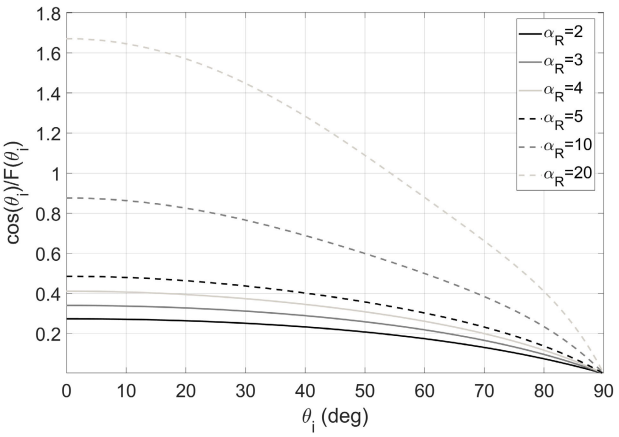

Fig. 5. Evaluation of the reciprocity of the legacy ER model.

it is valid only for surface roughness of the Gaussian type, with correlation length larger than the wavelength, and it also has approximations that make it invalid for grazing incidence angles, as discussed for instance in [30].

The Kirchhoff's scattering coefficient provided in [17] is composed of two parts, a coherent specular component, derived from the radar cross section theory, and an incoherent diffuse component which accounts for the nonspecular contribution of the facets representing the irregular surface. For the sake of comparison with the RER model, in the following we consider only the incoherent component. In Fig. 7, the normalized scattering diagrams for the RER model and the Kirchhoff model (diffuse incoherent component) are compared for a 1.3-GHz incident plane wave with $\theta_i = \pi/3$, the same case of [4, Fig. 10]. The following parameters are used in the Kirchhoff model: surface roughness standard deviation $\sigma_h = 1$ cm and correlation length $l_{corr} = 0.5$ m, which are typical literature values for a brick wall as the one considered in [4]. For comparison, the directivity parameter α_R of the RER model has been optimized to reproduce the same scattering lobe width as the Kirchhoff model, thus getting $\alpha_R = 65$, which is a much higher value with respect to what is found in [4] for the brick wall case, i.e., $\alpha_R = 4$. The shapes of the two patterns are very similar: interestingly, the maximum is slightly tilted upward with respect to the specular direction in both the cases, albeit to a lesser extent in the RER model case. However, the much greater degree of spreading observed in [4] is an indication that surface elements such as indentations and material inhomogeneities (e.g., the alternation of brick and mortar, and cavities inside bricks) probably give a greater contribution to DS than mere Gaussian surface roughness. Besides the aforementioned limitations, there are additional issues that make not straightforward the implementation of the Kirchhoff model in ray-based prediction tools, as discussed, for example, in [31]. Moreover, as the incoherent component is computed through a series expansion, the Kirchhoff model is computationally less efficient than the RER model, from 1 to 2 orders of magnitude depending on how the series is truncated.

Another possible approach to deal with DS from irregular surfaces is the one based on the use of computer graphics models, originally conceived for rendering of photorealistic images. Such models are based on the so-called bidirectional reflectance distribution function (BRDF), which is a directional scattering coefficient. In recent years, "physically based" BDRFs have been proposed, which obey reciprocity and comply with upper bound power constraints, such as that P_i should always be greater than or equal to P_s [27].

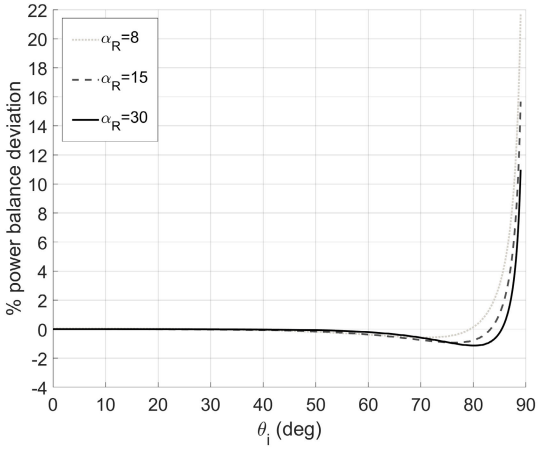

Fig. 6. Percentage deviation of the reciprocal model with respect to legacy power balance, normalized to the incident power.

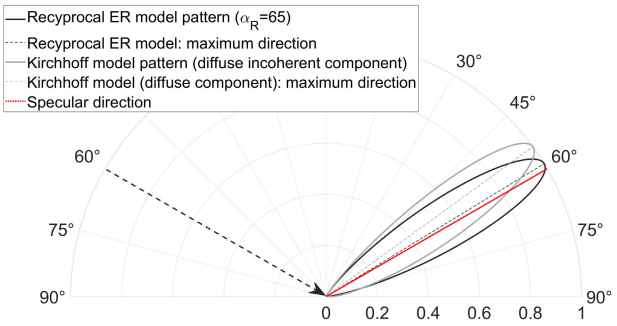

Fig. 7. Comparison between Kirchhoff's DS pattern for a brick wall at 1.3 GHz and best-fit RER DS pattern ($\theta_i = 45°$).

One example is the popular GGX shading model, originally introduced in [28]. In [29], it has been proposed to use a slightly modified version of the GGX model for radio wave propagation prediction. In the model, an equivalent roughness parameter Σ_s, expressed in dB, is used: $\Sigma_s = 0$ dB means maximum roughness, while $\Sigma_s < -40$ dB means smooth surface with quasi-specular behavior. In particular, in [29] it is shown that by parameterizing the GGX model to reproduce both the specular and diffuse components and by adding them through incoherent power sum, realistic results in good agreement with the measurements can be achieved.

In Fig. 8, the directional coefficient D of the GGX model as defined in [29] is compared with the scattering patterns of the RER model and the legacy ER model for an incidence angle $\theta_i = 45°$ and a surface with moderate roughness, i.e., $\Sigma_s = -4$ dB. In such a case, the best-fit directivity parameter is $\alpha_R = 8$ for both the RER and legacy ER models. The GGX and legacy ER models have a very similar scattering diagram, and interestingly both of them do not go to zero at grazing scattering angles, differently from the RER and the Kirchhoff models.

B. Comparison With Measurements

Finally, the new ER model is compared with the measurements carried out in [4] on three different reference scenarios: the façade of a rural building, a warehouse with brick walls, and a metal hangar wall of an airport. In the

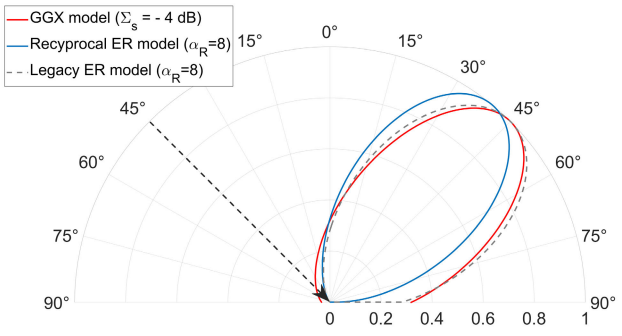

Fig. 8. Comparison between GGX computer graphics model, RER model, and legacy ER model for a surface with moderate roughness and $\theta_i = 45°$.

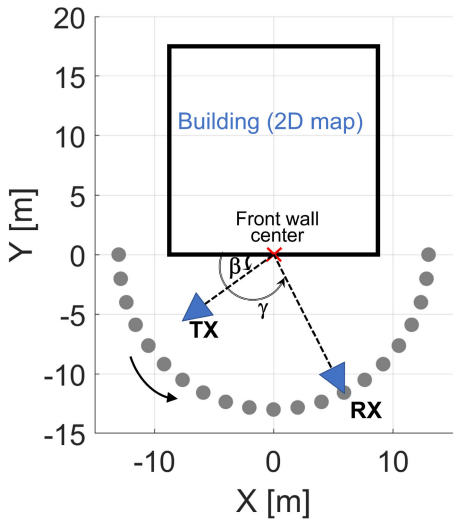

Fig. 9. 2-D view of the measurement scenario described in [4].

measurements, the façade of the building was illuminated by a Tx directive antenna pointing toward the center of the wall, while the Rx directive antenna, also aiming at the wall center, was moved along a semicircle in front of the wall to derive an estimate of the angular scattering pattern. A 2-D view of the measurement scenario is depicted in Fig. 9, where β and γ stand for the pointing angles of the Tx and Rx antennas, respectively.

Despite the use of directive antennas, all the interaction mechanisms (direct path, specular reflection, diffraction, DS) are simultaneously present to some extent, and therefore, the measured pattern needs to be compared with RT simulations including all the mechanisms: the new RER model has been embedded in the RT simulator described in [6], similar to what is done in [4] for the legacy model. Both parameters S and α_R have been optimized by varying their values over the range [0, 1] for S and [1, 20] for α_R with steps of 0.01 and 0.5, respectively, using a least-squares method to get the best match of the overall RT-simulated scattering pattern with the measured scattering pattern. The results are shown in Fig. 10 for the rural building case with slanted illumination (i.e., $\beta = 150°$): the optimum values of the parameters are $S = 0.36$ and $\alpha_R = 2$ in this case. As expected, the scattering model allows to fill the gap for those receiving positions where the coherent interaction mechanisms (specular

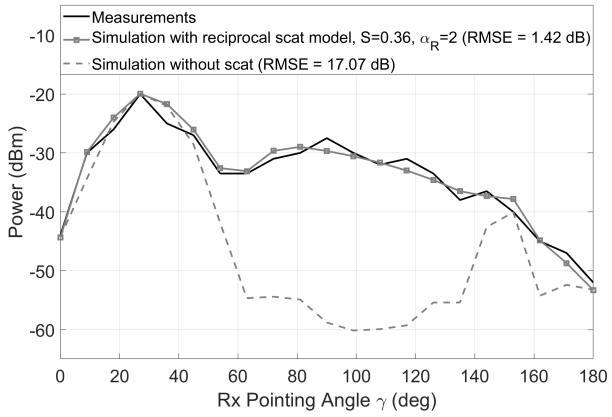

Fig. 10. Comparison between RT simulation with the RER DS model embedded and measurements in a rural building scenario (case of slanted Tx illumination, $\beta = 150°$).

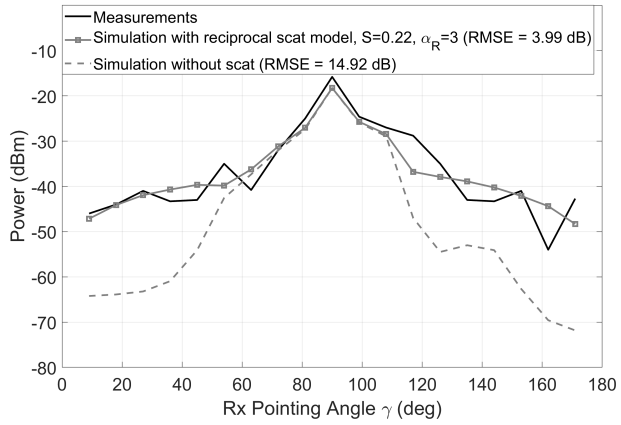

Fig. 11. Comparison between RT simulation with the RER DS model embedded and scattering measurements from a brick wall (case of normal Tx illumination, $\beta = 90°$).

reflection, diffraction) are weaker. The curve corresponding to a simulation without DS (i.e., $S = 0$) is also reported for reference in the figure and shows a very poor performance for the Rx locations further from the specular reflection angle (i.e., $\gamma = 30°$ in Fig. 10). From the plot, it is evident that the proposed model, if properly parameterized, can accurately describe scattering from such a typical building wall, with a root mean square error (RMSE) of 1.42 dB. This result is even better than the one shown in [4] for the legacy ER model in the same scenario, not reported in the figure for the sake of legibility, where the best RMSE value was 1.85 dB.

Similar results are shown in Figs. 11 and 12 for the brick wall (normal illumination, $\beta = 90°$) and hangar wall (slanted illumination, $\beta = 30°$), respectively. Also in these cases, the introduction of the RER model into the RT simulation allows a considerable reduction of the RMSE.

Finally, results for all the scenarios and illumination angles shown in [4] are summarized in Table I, showing the optimum values of S and α_R to achieve the best matching between measurements and simulation, and the obtained RMSE value. The RMSE value for the case $S = 0$ (no scattering in the RT simulation) is also reported for reference in the table. In all

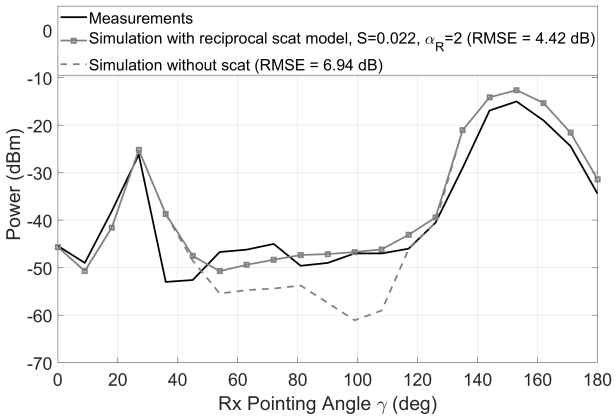

Fig. 12. Comparison between RT simulation with the RER DS model embedded and scattering measurements from a hangar wall (case of slanted Tx illumination, $\beta = 30°$).

TABLE I
OPTIMUM PARAMETERS FOR THE RER MODEL IN THE MEASUREMENT SCENARIOS AND RMSE OF SIMULATIONS WITH RESPECT TO MEASUREMENTS

Measurement scenario	Opt. S	Opt. α_R	RMSE (dB)	RMSE(dB) (S=0)
Hangar wall ($\beta = 90°$)	0.026	2	**2.97**	8.95
Hangar wall ($\beta = 30°$)	0.022	2	**4.42**	6.94
Brick wall ($\beta = 90°$)	0.22	3	**3.99**	14.92
Brick wall ($\beta = 150°$)	0.15	2	**2.8**	9.55
Rural building ($\beta = 90°$)	0.79	2	**1.92**	26.58
Rural building ($\beta = 150°$)	0.36	2	**1.42**	17.07

the cases, the results are similar or better than the ones shown in [4] for the legacy ER model.

Regarding the S parameter, it is confirmed that typical values for a metal wall, representative of relatively smooth surfaces, are below 0.1. In the case of medium roughness, such as the brick wall analyzed here, typical S values are around 0.2. In the case of a building façade with surface and volume irregularities, as for the rural building considered here, typical S values are 0.3–0.4. The optimum S value shown in Table I for the rural building with normal illumination is actually higher (0.79); however, by setting $S = 0.4$, the RMSE would increase only to 5 dB, still much better than the RMSE value for $S = 0$, which is 26.58 dB.

Moreover, in all the analyzed cases, it is confirmed that low values of α_R parameter, i.e., $\alpha_R = 2$ or $\alpha_R = 3$, are needed to achieve a good matching with measurements, also in agreement with other studies [7].

IV. CONCLUSION

The ER model, a popular model for DS from objects and building walls that is conceived to complement ray-based radio propagation models, is reconsidered and modified in the present work to satisfy reciprocity, an important physical-soundness requisite. To this aim, the formulation of the original model has been modified to satisfy reciprocity without significantly affecting the simple and yet sound power-balance approach it is based on. The new, reciprocal version of the ER model, which can be easily implemented and can replace the old version in ray-based propagation models, is analyzed

and compared with the old one and with other popular models in Section III. Finally, comparison with some of the measurements previously considered in [4] for the validation of the original model has shown that the new model yields similar performance, if not better.

APPENDIX A
EULER'S GAMMA AND BETA FUNCTIONS

The *Euler's Gamma function* definition is [32]

$$\Gamma(z) = \int_0^\infty t^{z-1}\, e^{-t}\, dt \tag{23}$$

where z is a complex number having positive nonzero real part ($\Re(z) > 0$). We recap here some useful properties of the Gamma function that will be used in the proofs of the next appendixes

$$\Gamma(z) = \frac{\Gamma(z+1)}{z} \tag{24}$$

$$\Gamma(z)\Gamma\left(z+\frac{1}{2}\right) = 2^{1-2z}\sqrt{\pi}\ \Gamma(2z) \tag{25}$$

$$\Gamma(n+1) = n! \tag{26}$$

$$\Gamma\left(\frac{n}{2}\right) = \frac{(n-2)!!}{2^{\frac{n-1}{2}}} \tag{27}$$

where n is a natural number, and $n!$, $n!!$ are the factorial and double factorial (or semi-factorial) functions, respectively, defined as

$$\begin{aligned} n! &= \prod_{k=0}^{n-1}(n-k) = n(n-1)(n-2)\dots \\ n!! &= \prod_{k=0}^{\lceil \frac{n}{2} \rceil - 1}(n-2k) = n(n-2)(n-4)\dots \end{aligned} \tag{28}$$

where $\lceil x \rceil$ stands for the least integer greater than or equal to x. Also, it is conventionally assumed $0! = 1$ and $0!! = 1$.

In the following appendixes, we will also make use of the following *binomial theorem* [32]:

$$(a+b)^n = \sum_{k=0}^{n}\binom{n}{k} a^{n-k}\, b^k = \sum_{k=0}^{n}\binom{n}{k} a^k\, b^{n-k} \tag{29}$$

where

$$\binom{n}{k} = \frac{n!}{k!\,(n-k)!}.$$

In the particular case that b is equal to the constant function $b(x) = 1$, (29) reduces to

$$(1+a)^n = \sum_{k=0}^{n}\binom{n}{k} a^k. \tag{30}$$

The *Euler's Beta function* is defined as [32]

$$B(x,y) = \int_0^1 t^{x-1}\,(1-t)^{y-1}\, dt \tag{31}$$

where $\Re(x) > 0$, $\Re(y) > 0$. The following properties hold:

$$B(x,y) = \frac{\Gamma(x)\Gamma(y)}{\Gamma(x+y)} \tag{32}$$

$$B(x,y) = 2\int_0^{\pi/2} \sin^{2x-1} t\ \cos^{2y-1} t\ dt. \tag{33}$$

APPENDIX B
COMPLETE DERIVATION OF F_{α_R} FOR THE LEGACY ER MODEL (NONRECIPROCAL)

The aim of this section is to prove (13), which is the closed-form solution of the integral (8) for the single-lobe scattering pattern of the legacy ER model [see (10)], originally proposed in [4]. The integral to be solved is

$$F_{\alpha_R} = \int_0^{2\pi}\int_0^{\pi/2}\left(\frac{1+\cos\psi_R}{2}\right)^{\alpha_R} \sin\theta_S\, d\theta_S\, d\phi_S \tag{34}$$

with $\cos\psi_R = \cos\theta_i\cos\theta_S - \sin\theta_i\sin\theta_S\cos(\phi_S - \phi_i)$. Using the binomial theorem in the form (29), we obtain

$$F_{\alpha_R} = \frac{1}{2^{\alpha_R}}\int_0^{2\pi}\int_0^{\pi/2}\sum_{j=0}^{\alpha_R}\binom{\alpha_R}{j}\cos^j\psi_R\,\sin\theta_S\, d\theta_S\, d\phi_S. \tag{35}$$

It follows that

$$\begin{aligned} F_{\alpha_R} = \frac{1}{2^{\alpha_R}}\sum_{j=0}^{\alpha_R}\binom{\alpha_R}{j}\int_0^{2\pi}\int_0^{\pi/2}(\cos\theta_i\cos\theta_S + \\ -\sin\theta_i\sin\theta_S\cos(\phi_S-\phi_i))^j\sin\theta_S\, d\theta_S\, d\phi_S. \end{aligned} \tag{36}$$

By applying the binomial theorem again [see (30)], we get

$$\begin{aligned} F_{\alpha_R} = \frac{1}{2^{\alpha_R}}\sum_{j=0}^{\alpha_R}\binom{\alpha_R}{j}\sum_{l=0}^{j}\binom{j}{l}(-1)^l\cos^{j-l}\theta_i\sin^l\theta_i \\ \cdot\int_0^{2\pi}\int_0^{\pi/2}\cos^{j-l}\theta_S\sin^l\theta_S\cos^l(\phi_S-\phi_i) \\ \cdot\sin\theta_S\, d\theta_S\, d\phi_S. \end{aligned} \tag{37}$$

Let I stand for

$$\begin{aligned} I &= \int_0^{2\pi}\int_0^{\pi/2}\cos^{j-l}\theta_S\sin^l\theta_S\cos^l(\phi_S-\phi_i)\sin\theta_S\, d\theta_S\, d\phi_S \\ &= \int_0^{\pi/2}\cos^{j-l}\theta_S\sin^{l+1}\theta_S\, d\theta_S\int_0^{2\pi}\cos^l(\phi_S-\phi_i)\, d\phi_S \\ &= I_1\cdot I_2. \end{aligned} \tag{38}$$

Let us consider the first factor in (38), i.e., $I_1 = \int_0^{\pi/2}\cos^{j-l}\theta_S\sin^{l+1}\theta_S\, d\theta_S$. Applying (33), we obtain

$$I_1 = \frac{1}{2}B\left(\frac{l}{2}+1, \frac{j-l+1}{2}\right). \tag{39}$$

The second factor $I_2 = \int_0^{2\pi}\cos^l(\phi_S-\phi_i)\, d\phi_S$ may be written as

$$I_2 = \int_0^{2\pi}(\cos\phi_S\cos\phi_i + \sin\phi_S\sin\phi_i)^l\, d\phi_S. \tag{40}$$

Using the binomial theorem, we get

$$I_2 = \sum_{q=0}^{l}\binom{l}{q}\cos^{l-q}\phi_i\sin^q\phi_i\int_0^{2\pi}\cos^{l-q}\phi_S\sin^q\phi_S\, d\phi_S. \tag{41}$$

Let $X = \int_0^{2\pi} \cos^{l-q}\phi_S \sin^q \phi_S \, d\phi_S$. This integral can be split into four parts

$$\begin{aligned} X = &\int_0^{\pi/2} \cos^{l-q}\phi_S \sin^q \phi_S \, d\phi_S \\ &+ \int_{\pi/2}^{\pi} \cos^{l-q}\phi_S \sin^q \phi_S \, d\phi_S \\ &+ \int_{\pi}^{3\pi/2} \cos^{l-q}\phi_S \sin^q \phi_S \, d\phi_S \\ &+ \int_{3\pi/2}^{2\pi} \cos^{l-q}\phi_S \sin^q \phi_S \, d\phi_S. \end{aligned} \tag{42}$$

It is evident that if q is odd, the four terms cancel each other out. The same thing happens when q is even and l is odd. On the other hand, when l and q are both even, the four terms give the same value. Therefore, we have

$$X = \begin{cases} 4\int_0^{\pi/2} \cos^{l-q}\phi_S \sin^q \phi_S \, d\phi_S, & \text{if } l,q \text{ even} \\ 0, & \text{otherwise.} \end{cases} \tag{43}$$

Using (33), we obtain

$$X = \begin{cases} 2B\left(\frac{q+1}{2}, \frac{l-q+1}{2}\right), & \text{if } l,q \text{ even} \\ 0, & \text{otherwise.} \end{cases} \tag{44}$$

Combining (37)–(39) and (41), we can assert that

$$\begin{aligned} F_{\alpha_R} = &\frac{1}{2^{\alpha_R}} \sum_{j=0}^{\alpha_R} \binom{\alpha_R}{j} \sum_{l=0}^{j} \binom{j}{l} (-1)^l \cos^{j-l}\theta_i \sin^l \theta_i \\ &\cdot \frac{1}{2} B\left(\frac{l}{2}+1, \frac{j-l+1}{2}\right) \sum_{q=0}^{l} \binom{l}{q} \cos^{l-q}\phi_i \sin^q \phi_i \, X. \end{aligned} \tag{45}$$

Since X is nonzero only when the indices l and q are even, combining (44) and (45), we can write

$$\begin{aligned} F_{\alpha_R} = &\frac{1}{2^{\alpha_R}} \sum_{j=0}^{\alpha_R} \binom{\alpha_R}{j} \sum_{l=0}^{\lfloor j/2 \rfloor} \binom{j}{2l} \cos^{j-2l}\theta_i \sin^{2l}\theta_i \\ &\cdot B\left(l+1, \frac{j-2l+1}{2}\right) \sum_{q=0}^{l} \binom{2l}{2q} \cos^{2l-2q}\phi_i \sin^{2q}\phi_i \\ &\cdot B\left(q+\frac{1}{2}, l-q+\frac{1}{2}\right). \end{aligned} \tag{46}$$

Let us consider $B(l+1, ((j-2l+1)/2))$ and $B(q+(1/2), l-q+(1/2))$. Using properties (26), (27), and (32), it is simple to obtain

$$B\left(l+1, \frac{j-2l+1}{2}\right) = 2^{l+1} l! \frac{(j-2l-1)!!}{(j+1)!!}. \tag{47}$$

In a similar way, using (25), (27), and (32), we get

$$B\left(q+\frac{1}{2}, l-q+\frac{1}{2}\right) = \frac{\pi (2q)!(2l-2q)!}{2^{2l} q! \, l!(l-q)!}. \tag{48}$$

By substituting (47) and (48) into (46) and rearranging some terms, we obtain

$$\begin{aligned} F_{\alpha_R} = &\frac{2\pi \, \alpha_R!}{2^{\alpha_R}} \sum_{j=0}^{\alpha_R} \frac{1}{(\alpha_R - j)!(j+1)!!} \sum_{l=0}^{\lfloor j/2 \rfloor} \frac{\cos^{j-2l}\theta_i \sin^{2l}\theta_i}{2^l (j-2l)!!} \\ &\cdot \sum_{q=0}^{l} \frac{\cos^{2l-2q}\phi_i \sin^{2q}\phi_i}{q!(l-q)!} \end{aligned} \tag{49}$$

where the symbol $\lfloor x \rfloor$ stands for the greatest integer less than or equal to x.

But $\sum_{q=0}^{l} (\cos^{2l-2q}\phi_i \sin^{2q}\phi_i)/(q!(l-q)!)$ equals $1/l!$, as it can be easily verified by applying the binomial theorem. Then, after this substitution we can eventually write the final formulation of F_{α_R}

$$F_{\alpha_R} = \frac{2\pi \, \alpha_R!}{2^{\alpha_R}} \sum_{j=0}^{\alpha_R} \frac{1}{(\alpha_R - j)!(j+1)!!} \sum_{l=0}^{\lfloor j/2 \rfloor} \frac{\cos^{j-2l}\theta_i \sin^{2l}\theta_i}{2^l \, l!(j-2l)!!}. \tag{50}$$

This equation is also valid in the case of normal incidence, i.e., $\theta_i = 0$, if for the 0^{th}-order term of the second summation it is *conventionally* assumed, as most automatic calculators do:

$$\lim_{\theta_i \to 0} (\sin\theta_i)^0 = 0^0 = 1.$$

In such a case, for normal incidence (50) reduces to

$$F_{\alpha_R}(0) = \frac{4\pi}{\alpha_R + 1}\left(1 - \frac{1}{2^{\alpha_R+1}}\right).$$

The same result can also be obtained by directly integrating (8) for $\theta_i = 0$, which is straightforward.

Appendix C
Solution of the Power-Balance Integral for the New ER Reciprocal Model (Single-Lobe Version)

The aim of this section is to justify (17). We assume that F_{α_R} can be written in the following, approximate form, as discussed in Section II:

$$F_{\alpha_R} \approx k(\alpha_R)\sqrt{\cos\theta_i}. \tag{51}$$

Looking at this expression, we observe that $k(\alpha_R)$ is equal to F_{α_R} when $\theta_i = 0$. Thus, we can assert that

$$F_{\alpha_R} \approx k(\alpha_R)\sqrt{\cos\theta_i} = F_{\alpha_R}(\theta_i = 0)\sqrt{\cos\theta_i}. \tag{52}$$

The value of $F_{\alpha_R}(\theta_i = 0)$ can be found by directly integrating (8) for $\theta_i = 0$, and observing that, for normal incidence, $\cos\psi_R = \cos\theta_S$. Then, we get

$$F_{\alpha_R} \approx \frac{2\pi\sqrt{\cos\theta_i}}{2^{\alpha_R}} \int_0^{\frac{\pi}{2}} \sqrt{\cos\theta_S}(1+\cos\theta_S)^{\alpha_R} \sin\theta_S \, d\theta_S. \tag{53}$$

Then, by applying the binomial theorem, we obtain

$$F_{\alpha_R} \approx \frac{2\pi\sqrt{\cos\theta_i}}{2^{\alpha_R}} \int_0^{\frac{\pi}{2}} \sin\theta_S \sqrt{\cos\theta_S} \sum_{j=0}^{\alpha_R} \binom{\alpha_R}{j} \cos^j\theta_S \, d\theta_S. \tag{54}$$

Equation (54) can be rewritten as

$$F_{\alpha_R} \approx \frac{2\pi\sqrt{\cos\theta_i}}{2^{\alpha_R}} \sum_{j=0}^{\alpha_R} \binom{\alpha_R}{j} \int_0^{\frac{\pi}{2}} \sin\theta_S \cos^{j+\frac{1}{2}}\theta_S \, d\theta_S. \quad (55)$$

Applying (33) in (55), we have

$$F_{\alpha_R} \approx \frac{\pi\sqrt{\cos\theta_i}}{2^{\alpha_R}} \sum_{j=0}^{\alpha_R} \binom{\alpha_R}{j} B\left(1, \frac{j}{2}+\frac{3}{4}\right). \quad (56)$$

Using properties (24) and (32), we get the final expression for F_{α_R}:

$$F_{\alpha_R} \approx \frac{4\pi\sqrt{\cos\theta_i}}{2^{\alpha_R}} \sum_{j=0}^{\alpha_R} \binom{\alpha_R}{j} \frac{1}{2j+3}. \quad (57)$$

Eventually, (17) is obtained by substituting (14) and (57) into (7).

Appendix D
Solution of the Power-Balance Integral for the Double-Lobe RER Model

The aim of this section is to justify (20). To do that, let us consider the two integrals in (19)

$$F_{\alpha_R} = \int_0^{2\pi}\int_0^{\frac{\pi}{2}} \sqrt{\cos\theta_S}\left(\frac{1+\cos\psi_R}{2}\right)^{\alpha_R} \sin\theta_S d\theta_S d\phi_S$$
$$F_{\alpha_i} = \int_0^{2\pi}\int_0^{\frac{\pi}{2}} \sqrt{\cos\theta_S}\left(\frac{1+\cos\psi_i}{2}\right)^{\alpha_i} \sin\theta_S d\theta_S d\phi_S \quad (58)$$

and remember that [4]

$$\cos\psi_i = \cos\theta_i\cos\theta_S + \sin\theta_i\sin\theta_S\cos(\phi_S-\phi_i). \quad (59)$$

We note that the only difference between (11) and (59) is in the sign of the second term.

We want to show that the integrals in (58) have the same result, for a fixed value of the exponent. Proving this is equivalent to proving that the result of the integral M defined in (60) does not depend on the sign of the term $\sin\theta_i\sin\theta_S\cos(\phi_S-\phi_i)$

$$M = \int_0^{2\pi}\int_0^{\pi/2} \sqrt{\cos\theta_S}(1+\cos\theta_i\cos\theta_S + \pm\sin\theta_i\sin\theta_S\cos(\phi_S-\phi_i))^m \sin\theta_S\, d\theta_S\, d\phi_S. \quad (60)$$

To prove that, we apply the binomial theorem twice and with a little manipulation of the factors, we get

$$M = \sum_{j=0}^{m}\binom{m}{j}\sum_{l=0}^{j}\left[\binom{j}{l}(\pm1)^l \sin^l\theta_i\cos^{j-l}\theta_i \cdot \int_0^{\pi/2}\sin^{l+1}\theta_S\cos^{j-l+\frac{1}{2}}\theta_S\, d\theta_S \cdot \int_0^{2\pi}\cos^l(\phi_S-\phi_i)^{\alpha_R}\sin\theta_S\, d\phi_S\right]. \quad (61)$$

But $\int_0^{2\pi}\cos^l(\phi_S-\phi_i)^{\alpha_R}\sin\theta_S\, d\phi_S \neq 0$ only when the index l is even. Thus, the overall contribution of the term $(\pm1)^l$ is completely irrelevant since $(+1)^l = (-1)^l = 1$ when l is even. This proves that the $\pm$ sign does not change the result of M.

Therefore, the two integrals in (58) have the same form, and the only difference between them is in the value of the exponent, either α_R or α_i. By adopting the same procedure as in Appendix C, we then find that

$$F_{\alpha_R} \approx F_{\alpha_R}(0)\sqrt{\cos\theta_i} \approx \frac{4\pi\sqrt{\cos\theta_i}}{2^{\alpha_R}}\sum_{j=0}^{\alpha_R}\binom{\alpha_R}{j}\frac{1}{2j+3}$$
$$F_{\alpha_i} \approx F_{\alpha_i}(0)\sqrt{\cos\theta_i} \approx \frac{4\pi\sqrt{\cos\theta_i}}{2^{\alpha_i}}\sum_{j=0}^{\alpha_i}\binom{\alpha_i}{j}\frac{1}{2j+3} \quad (62)$$

and by substituting $F_{\alpha_i,\alpha_R} = \Lambda F_{\alpha_R} + (1-\Lambda)F_{\alpha_i}$ into (18), we finally get (20).

References

[1] L. Felsen and N. Marcuvitz, *Radiation and Scattering of Waves*. New York, NY, USA: IEEE Press, 1973.

[2] V. Degli-Esposti and H. L. Bertoni, "Evaluation of the role of diffuse scattering in urban microcellular propagation," in *Proc. 21st Century Commun. Village, VTC-Fall, IEEE VTS 50th Veh. Technol. Conf.*, May 1999, pp. 1392–1396.

[3] V. Degli-Esposti, "A diffuse scattering model for urban propagation prediction," *IEEE Trans. Antennas Propag.*, vol. 49, no. 7, pp. 1111–1113, Jul. 2001.

[4] V. Degli-Esposti, F. Fuschini, E. M. Vitucci, and G. Falciasecca, "Measurement and modelling of scattering from buildings," *IEEE Trans. Antennas Propag.*, vol. 55, no. 1, pp. 143–153, Jan. 2007.

[5] E. M. Vitucci, J. Chen, V. Degli-Esposti, J. S. Lu, H. L. Bertoni, and X. Yin, "Analyzing radio scattering caused by various building elements using millimeter-wave scale model measurements and ray tracing," *IEEE Trans. Antennas Propag.*, vol. 67, no. 1, pp. 665–669, Jan. 2019.

[6] V. Degli-Esposti, D. Guiducci, A. de'Marsi, P. Azzi, and F. Fuschini, "An advanced field prediction model including diffuse scattering," *IEEE Trans. Antennas Propag.*, vol. 52, no. 7, pp. 1717–1728, Jul. 2004.

[7] F. Mani, F. Quitin, and C. Oestges, "Directional spreads of dense multipath components in indoor environments: Experimental validation of a ray-tracing approach," *IEEE Trans. Antennas Propag.*, vol. 60, no. 7, pp. 3389–3396, Jul. 2012.

[8] E. M. Vitucci, F. Mani, V. Degli-Esposti, and C. Oestges, "Polarimetric properties of diffuse scattering from building walls: Experimental parameterization of a ray-tracing model," *IEEE Trans. Antennas Propag.*, vol. 60, no. 6, pp. 2961–2969, Jun. 2012.

[9] F. Mani, E. M. Vitucci, F. Quitin, V. Degli-Esposti, and C. Oestges, "Parameterization of a polarimetric diffuse scattering model in indoor environments," *IEEE Trans. Antennas Propag.*, vol. 62, no. 8, pp. 4361–4364, Aug. 2014.

[10] E. M. Vitucci, L. Tarlazzi, F. Fuschini, P. Faccin, and V. Degli-Esposti, "Interleaved-MIMO DAS for indoor radio coverage: Concept and performance assessment," *IEEE Trans. Antennas Propag.*, vol. 62, no. 6, pp. 3299–3309, Jun. 2014.

[11] V. Degli-Esposti et al., "Ray-tracing-based mm-wave beamforming assessment," *IEEE Access*, vol. 2, pp. 1314–1325, 2014.

[12] F. Fuschini, M. Zoli, E. M. Vitucci, M. Barbiroli, and V. Degli-Esposti, "A study on millimeter-wave multiuser directional beamforming based on measurements and ray tracing simulations," *IEEE Trans. Antennas Propag.*, vol. 67, no. 4, pp. 2633–2644, Apr. 2019.

[13] E. M. Vitucci et al., "Tuning ray tracing for mm-wave coverage prediction in outdoor urban scenarios," *Radio Sci.*, vol. 54, no. 11, pp. 1112–1128, Nov. 2019.

[14] F. Sheikh, Y. Gao, and T. Kaiser, "A study of diffuse scattering in massive MIMO channels at terahertz frequencies," *IEEE Trans. Antennas Propag.*, vol. 68, no. 2, pp. 997–1008, Feb. 2020.

[15] P. Xie, K. Guan, D. He, H. Yi, J. Dou, and Z. Zhong, "Terahertz wave propagation characteristics on rough surfaces based on full-wave simulations," *Radio Sci.*, vol. 57, no. 6, pp. 1–16, Jun. 2022.

[16] C. Jansen et al., "Diffuse scattering from rough surfaces in THz communication channels," *IEEE Trans. Terahertz Sci. Technol.*, vol. 1, no. 2, pp. 462–472, Nov. 2011.

[17] P. Beckmann and A. Spizzichino, *The Scattering of Electromagnetic Waves From Rough Surfaces*. Oxford, U.K.: Pergamon Press, 1963.

[18] L. Tsang, J. Kong, and K.-H. Ding, *Scattering of Electromagnetic Waves: Theories and Applications*. Hoboken, NJ, USA: Wiley, 2000.
[19] P. Pongsilamanee and H. L. Bertoni, "Specular and nonspecular scattering from building facades," *IEEE Trans. Antennas Propag.*, vol. 52, no. 7, pp. 1879–1889, Jul. 2004.
[20] V. Degli-Esposti, F. Fuschini, and E. M. Vitucci, "A fast model for distributed scattering from buildings," in *Proc. 3rd Eur. Conf. Antennas Propag.*, 2009, pp. 1932–1936.
[21] F. Fuschini, V. Degli-Esposti, and E. M. Vitucci, "A model for forward-diffuse scattering through a wall," in *Proc. 4th Eur. Conf. Antennas Propag.*, 2010, pp. 1–4.
[22] L. Minghini, R. D'Errico, V. Degli Esposti, and E. M. Vitucci, "Electromagnetic simulation and measurement of diffuse scattering from building walls," in *Proc. 8th Eur. Conf. Antennas Propag. (EuCAP)*, Apr. 2014, pp. 1298–1302.
[23] J. Pascual-García, J. Molina-García-Pardo, M. Martínez-Inglés, J. Rodríguez, and N. Saurín-Serrano, "On the importance of diffuse scattering model parameterization in indoor wireless channels at mm-wave frequencies," *IEEE Access*, vol. 4, pp. 688–701, 2016.
[24] F. Fuschini et al., "Item level characterization of mm-wave indoor propagation," *EURASIP J. Wireless Commun. Netw.*, vol. 2016, no. 1, pp. 1–10, Dec. 2016.
[25] Remcom. (2022). *Wireless InSite Diffuse Scattering*. Accessed: Sep. 8, 2022. [Online]. Available: https://www.remcom.com/wireless-insite-diffuse-scattering
[26] J. Van Bladel, *Electromagnetic Fields*. New York, NY, USA: Wiley, 2007, pp. 405–413.
[27] B. Duvenhage, K. Bouatouch, and D. G. Kourie, "Numerical verification of bidirectional reflectance distribution functions for physical plausibility," in *Proc. South Afr. Inst. Comput. Scientists Inf. Technologists Conf.*, Oct. 2013, pp. 200–208.
[28] B. Walter, S. R. Marschner, H. Li, and K. E. Torrance, "Microfacets models for refraction through rough surfaces," in *Proc. Eurograph. Symp. Rendering Techn. (EGSR)*, Grenoble, France, Jul. 2007.
[29] J.-F. Wagen, "Diffuse scattering and specular reflection from facets of arbitrary size and roughness using the computer graphics GGX model," in *Proc. Int. Symp. Netw., Comput. Commun. (ISNCC)*, 2020, pp. 1–5.
[30] M. Saillard and G. Soriano, "Rough surface scattering at low-grazing incidence: A dedicated model," *Radio Sci.*, vol. 46, no. 5, pp. 1–8, Oct. 2011.
[31] S. Priebe, M. Jacob, C. Jansen, and T. Kürner, "Non-specular scattering modeling for THz propagation simulations," in *Proc. 5th Eur. Conf. Antennas Propag. (EUCAP)*, 2011, pp. 1–5.
[32] M. Abramowitz and I. A. Stegun, *Handbook of Mathematical Functions With Formulas, Graphs, and Mathematical Tables*. New York, NY, USA: Dover, 1964.

Enrico M. Vitucci (Senior Member, IEEE) was a Visiting Researcher with Polaris Wireless, Inc., Mountain View, CA, USA, in 2015. He was a Research Associate with the Center for Industrial Research on ICT, University of Bologna, Bologna, Italy. He is currently an Associate Professor in applied electromagnetics, antennas, and propagation with the Department of Electrical, Electronic and Information Engineering "Guglielmo Marconi" (DEI), University of Bologna. He is also the Chair of the Cesena-Forli Unit, Inter-Department Center for Industrial Research on ICT (CIRI-ICT), University of Bologna. He is the author or a coauthor of about 100 technical articles on international journals and conferences and a co-inventor of five international patents. He has participated in several European research and cooperation programs (COST 2100, COST IC1004, COST IRACON, and COST INTERACT) and in the European Networks of Excellence NEWCOM and NEWCOM++. His research interests are in deterministic and wireless propagation models for 5G and beyond.

Prof. Vitucci is a member of the Editorial Board of the *Wireless Communications and Mobile Computing* journal.

Nicolò Cenni received the B.Sc. degree in electronic engineering from the University of Bologna, Cesena Campus, Bologna, Italy, in 2021. He is currently pursuing the M.Sc. degree in electronic and telecommunications engineering with the Department of Electrical, Electronic and Information Engineering (DEI), University of Bologna.

His research interests are in wireless communications, radio propagation, applied electromagnetics, and mathematics.

Mr. Cenni has received the Best B.Sc. Thesis in electronic engineering at the Cesena Campus and the scholarship funded by JMA Wireless Italy, Bologna.

Franco Fuschini received the M.Sc. degree in telecommunication engineering and the Ph.D. degree in electronics and computer science from the University of Bologna, Bologna, Italy, in March 1999 and July 2003, respectively.

He is currently an Associate Professor with the Department of Electrical, Electronic and Information Engineering "Guglielmo Marconi," University of Bologna. He is the author or a coauthor of more than 30 journal articles on radio propagation and wireless system design. His main research interests are in the areas of radio systems design and radio propagation channel theoretical modeling and experimental investigation.

Dr. Fuschini received the "Marconi Foundation Young Scientist Prize" in the context of the XXV Marconi International Fellowship Award in April 1999.

Vittorio Degli-Esposti (Senior Member, IEEE) was a Post-Doctoral Researcher with Polytechnic University (now NYU Polytechnic), Brooklyn, NY, USA, in 1998, in the group led by Professor H. L. Bertoni. He was an Adjunct Professor with the Helsinki University of Technology (now Aalto University), Espoo, Finland, and Tongji University, Shanghai, China, in 2006 and 2013, respectively. From January 2015 to December 2016, he was the Director of Research at Polaris Wireless Inc., Mountain View, CA, USA. He is currently an Associate Professor with the "Dipartimento di Ingegneria Elettrica, Elettronica e dell'Informazione" (DEI) of the Alma Mater Studiorum, University of Bologna, Bologna, Italy. He is qualified (Abilitazione S. N.) as a Full Professor. He has participated in several European Research Projects, including the European Cooperation Actions COST 231, 259, 273, 2100, IC1004, IRACON, and INTERACT; the European Networks of Excellence NEWCOM and NEWCOM++; and the Seventh Framework Program IP Project ALPHA. He has been the Founder and a Lecturer of the biennial courses for Ph.D. students and researchers "Short range radio propagation: theory, models and future applications" and "Mobile radio propagation for 5G and beyond" of the European School of Antennas (http://www.antennasvce.org/Community/Education/Courses/). He is the author or a coauthor of more than 140 peer-reviewed technical articles and a co-inventor of seven international patents in the fields of applied electromagnetics, radio propagation, and wireless systems.

Dr. Degli-Esposti was elected as the Chair of the Propagation Working Group (WG9) of the European Association on Antennas and Propagation (EuRAAP). He was the Vice-Chair of the European Conference on Antennas and Propagation (EuCAP), editions 2010 and 2011, the Short-Courses and Workshops Chair of the 2015 edition, an Invited Speaker at EuCAP 2014 and International Symposium on Antennas and Propagation (ISAP) 2020, and the Short-Courses Chair of the European Conference on Networks and Communications (EuCNC) 2020. He is an Editor of the IEEE TRANSACTIONS ON VEHICULAR TECHNOLOGY and an Associate Editor of the journals *Radio Science* and IEEE ACCESS.

Open Access funding provided by 'Alma Mater Studiorum - Università di Bologna' within the CRUI CARE Agreement